'Surfaces-as-ligands, surfaces-as-complexes' strategies for copper(I) dye-sensitized solar cells

Ewald Schönhofer, Biljana Bozic-Weber, Colin J. Martin, Edwin C. Constable,* Catherine E. Housecroft* and Jennifer A. Zampese

Department of Chemistry, University of Basel, Spitalstrasse 51, 4056-Basel, Switzerland

Fax: +41 61 267 1018; E-mail: catherine.housecroft@unibas.ch

Abstract

A series of TiO_2-supported copper(I) dyes, $[Cu(L_{anchor})(L_{ancillary})]^+$ with $L_{ancillary}$ = 2,2':4',4":2",2'"-quaterpyridine (**1**), 4,4'-bis(6-methyl-[2,2'-bipyridin]-4-yl)-1,1'-biphenyl (**2**), or 4,4'-bis(6,6'-dimethyl-[2,2'-bipyridin]-4-yl)-1,1'-biphenyl (**3**), and L_{anchor} = (6,6'-dimethyl-[2,2'-bipyridine]-4,4'-diyl)bis(4,1-phenylene)bis(phosphonic acid) (**4**), has been assembled in a stepwise manner. DSSCs incorporating these dyes demonstrate the need for 6,6'-substituents in both ligands in $[Cu(L_{anchor})(L_{ancillary})]^+$; both J_{SC} and V_{OC} increase on going from $[Cu(\mathbf{4})(\mathbf{1})]^+$ to $[Cu(\mathbf{4})(\mathbf{2})]^+$ to $[Cu(\mathbf{4})(\mathbf{3})]^+$. First, second and third generation dyes $[(\mathbf{4})\{Cu(\mathbf{3})\}_n]^{n+}$ (n = 1, 2 or 3) have been assembled using the 'surfaces-as-ligands, surfaces-as-complexes' strategy, although the separation between sites of electron injection and hole transporting domains in the multinuclear complexes fails to enhance DSSC performance. Replacing $L_{ancillary}$ **2** in $[Cu(\mathbf{4})(\mathbf{2})]^+$ by the metalloligand $\{Ru(bpy)_2(\mathbf{2})\}^{2+}$ improves dye performance due to the better spectral response of the heteronuclear $[Cu(\mathbf{4})\{(\mathbf{2})Ru(bpy)_2\}]^{3+}$ complex. This assembly approach presents a flexible method of tuning dye properties while retaining the surface-bound bis(diimine)copper(I) domain.

Keywords: copper; ruthenium; sensitizer; DSSC; surface-functionalization

1. Introduction

A proven approach for increasing the light-harvesting efficiency of dyes in dye-sensitized solar cells (DSSCs) is to mimic the strategies that Nature [1,2,3,4] has successfully adopted and use the 'antenna effect' in which electron- or energy-transfer between multiple metal centres results in enhanced photon harvesting [5]. A wide range of mononuclear ruthenium(II) complexes designed to exhibit an antenna effect has been reported, and recent examples include dyes from Falares [6,7], Wang [8], Chandrasekharam and De Angelis [9], El-Shafei [10] and Ko [11]. Despite the antenna effect being well-established in multinuclear oligopyridine complexes [12], only a few reports deal with the functionalization of TiO_2 and the construction of DSSCs using multinuclear complexes [13,14,15,16,17]. These typically comprise an anchored ruthenium(II) photosensitizer covalently attached to one or more second or third row d-block metal-containing domain or domains (for example, Scheme 1). Distinct from these types of dyes is a sensitizer featuring covalently linked $\{Ru^{II}(bpy)_2\}$ and $\{Cu^{II}(cyclam)\}$ units (Scheme 2) which achieves a photon-to-current efficiency of 2.55% versus 6.4% for the standard ruthenium dye N719 [18]. The choice of metal centres and of bridging and peripheral ligands in the complex is critical for ensuring the correct direction of electron and/or energy transfer. The dye should incorporate multiple visible light-absorbing domains and also be able to inject electrons into the semiconductor. Multinuclear dyes previously reported include those in Scheme 1 and their wedge-shaped geometry results in a footprint that is spatially challenged for surface-functionalization. In the case of the triruthenium dendron shown on the right of Scheme 1, physisorption of the highly charged dye is a problem and only low photocurrents were observed [14].

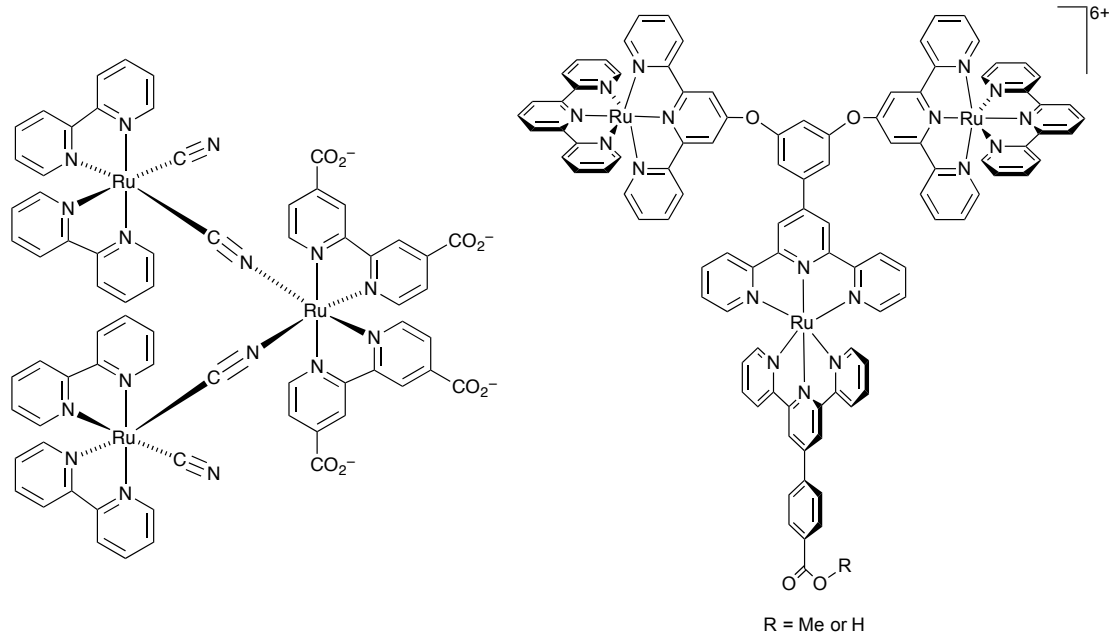

Scheme 1. Examples of multinuclear ruthenium(II) sensitizers [13,14] investigated as dyes in DSSCs.

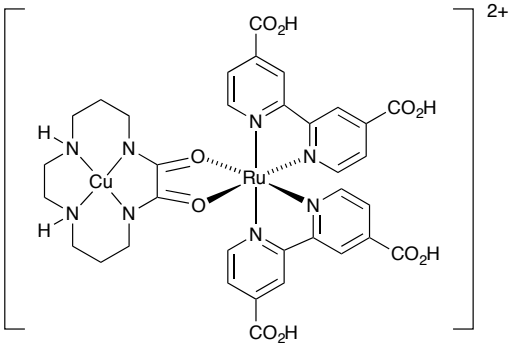

Scheme 2. A dinuclear ruthenium(II)–copper(II) sensitizer utilized as a dye in DSSCs [18].

Synthesis of structurally complex dyes prior to adsorption on a TiO_2 surface is time-consuming and gives no flexibility for ready tuning of the properties of the dye. Furthermore, uncertainties of the protonation state of the surface-binding modalities, typically carboxylic acid or phosphonic acid, are amplified in complexes containing two or more such functionalities resulting in the need for additional cycles in device

optimization. In order to optimize atom efficiency and to facilitate the screening of libraries of surface-bound dyes, we have developed methods of stepwise assembly of surface-bound bis(diimine) copper(I) dyes. In a further extention of the 'complexes-as-ligands' methodology introduced by the Bologna group for the systematic and regiospecific synthesis of homo- and heterometallic complexes [19,20], we have developed a powerful 'surfaces-as-ligands, surfaces-as-complexes' strategy for the preparation of DSSCs and other interfacial heterojunction devices [21,22,23,24,25,26,27,28]. In this approach, a nanoparticulate TiO_2 surface is treated with an anchoring ligand (L_{anchor}) which possesses two orthogonal functionalities: one is the anchoring group which interacts with the semiconductor (metal oxide in our case) surface and the other is one that can bind a metal centre. The interaction of the semiconductor with L_{anchor} gives a material with a surface-immobilized ligand, i.e. the 'surface-as-ligand' species. This material has the ligand covalently attached to the semiconductor surface through the carboxylate or phosphonate functionality, but at the same time exhibits an array of surface-bound but uncoordinated metal-binding groups which can be further addressed with appropriate metal centres. Immersion in a solution of a homoleptic copper(I) complex, $[Cu(L_{ancillary})_2]^+$, and ligand exchange between $L_{ancillary}$ and the surface-bound L_{anchor} gives the surface-bound complex $\{Cu(L_{anchor})(L_{ancillary})\}$ with a timescale of hours to days (Scheme 3a). The disadvantage of this method is that half of the $L_{ancillary}$ ligands in $[Cu(L_{ancillary})_2]^+$ are lost in this process, which limits the atom efficiency in the overall fabrication procedure. We have recently shown that DSSCs with efficiencies equal to those prepared in this manner can be fabricated by first functionalizing the FTO/TiO_2 electrode with L_{anchor}, subsequently treating with $[Cu(MeCN)_4][PF_6]$ to form a surface bound $\{(L_{anchor})CuX_2\}$ species, and finally with $L_{ancillary}$ to give $\{Cu(L_{anchor})(L_{ancillary})\}$ attached to the surface [29]. We now report the use

of this methodology for the assembly of different generation surface-bound copper(I) or copper(I)/ruthenium(II) dyes with multiple domains, and their performances in DSSCs. Both of these methods are optimized for the preparation of surface bound heteroleptic complexes for cases in which the solution phase complex cannot be isolated as a pure chemical species. We note that in the case of macrocyclic ligands and ligands bearing bulky substituents at the 6- and 6'-positions, the heteroleptic species can be isolated. In our case the surface immobilized ligand essentially removes the metal and the ancillary ligand from the virtual equilibrium. The two dye-assembly schemes are presented in Figure 1.

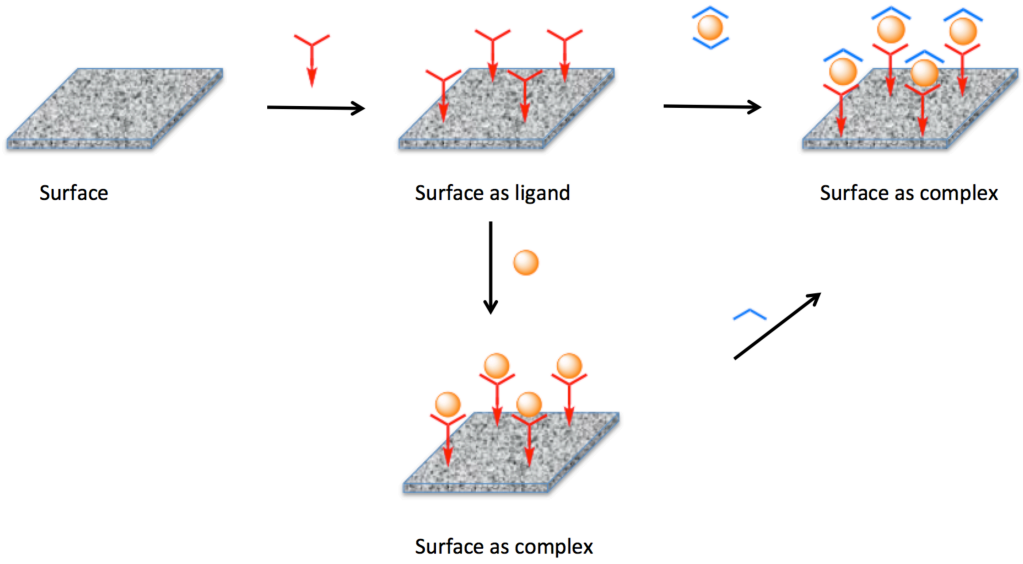

Figure 1. The two competing routes for stepwise assembly of photoactive dyes on a semiconductor surface. The first step in both cases is the irreversible attachment of an anchoring ligand (red) which contains a group which binds to the surface (the arrowhead) and a metal-binding domain to generate a 'surface-as-ligand'. In the upper route, this is then reacted with a homoleptic complex containing the ancillary ligands of choice to give the surface bound heteroleptic complex as a 'surface-as-complex'. The consequence of this is the loss of one equivalent of the ancillary ligand. The lower route shows the more atom economic version in which the 'surface-as-ligand' is first treated with a metal solvento-complex to give an intermediate 'surface-as-complex' with labile solvent ligands which is subsequently reacted with the ancillary ligand to generate the heteroleptic 'surface-as-'complex'.

2. Experimental

2.1 General

^{1}H and ^{13}C NMR spectra were recorded on a Bruker Avance III-500 NMR spectrometer; chemical shifts were referenced to residual solvent peaks with respect to ∂(TMS) = 0 ppm. Solution absorption spectra were recorded using a Cary 5000 or Agilent 8453 spectrophotometer, and FT-IR spectra using a Shimadzu 8400S spectrophotometer with Golden Gate attachment for solid samples. MALDI-TOF and electrospray ionization (ESI) mass spectra were recorded on Bruker esquire 3000^{plu} and Bruker Daltonics Inc. microflex instruments, respectively.

1-(2-Oxopropyl)pyridinium chloride [30], (*E*)-3-(4-bromophenyl)-1-(pyridin-2-yl)prop-2-en-1-one [31], (*E*)-3-(4-bromophenyl)-1-(6-methylpyrid-2-yl)prop-2-en-1-one [32], compound **4** [25], $[Cu(MeCN)_4][PF_6]$ [33] and *cis*-$[Ru(bpy)_2Cl_2]$ [34] were prepared by literature methods. The dye N791 was purchased from Solaronix. Zinc dust was purchased from Sigma-Aldrich; if not fresh, it required activation [35].

*2.2 2,2':4',4'':2'',2'''-Quaterpyridine (**1**)*

PPh_3 (4.51 g, 17.2 mmol) and $NiCl_2{\cdot}6H_2O$ (1.03 g, 4.3 mmol) were dissolved in DMF (25 mL) under N_2. Activated zinc powder (0.300 g, 4.3 mmol) was added and the mixture was heated to 50 ^{o}C and stirred for 1 h until it turned dark red. After stirring for another hour, 4-bromo-2,2'-bipyridine (1.02 g, 4.3 mmol) was added and the mixture stirred at 50 ^{o}C for 12 h. After cooling to room temperature, the reaction mixture was poured into aqueous NH_3 solution (150 mL, 32%) and then extracted with CH_2Cl_2 (3 × 50 mL). The organic phase was washed with water and dried over $MgSO_4$. The solvent was removed under reduced pressure and the crude product purified by column chromatography (silica,

MeOH/CH_2Cl_2, 1:99) and then recrystallized from EtOH. Compound **1** was isolated as a white solid which was dried under vacuum (130 mg, 0.419 mmol, 19%). Spectroscopic data were in accord with those reported [36].

2.3 4-(4-Bromophenyl)-6-methyl-2,2'-bipyridine

(*E*)-3-(4-Bromophenyl)-1-(pyridin-2-yl)prop-2-en-1-one (2.00 g, 6.94 mmol) was dissolved in MeOH (100 mL) and 1-(2-oxopropyl)pyridinium chloride (1.19 g, 6.94 mmol) was added. The mixture was treated with excess NH_4OAc (16.0 g, 208 mmol), heated at reflux for 24 h, then cooled to room temperature. It was then placed in a refrigerator overnight during which time a precipitate formed. This was collected by filtration, washed with H_2O (3 × 15 mL) and MeOH (3 × 15 mL) and dried under vacuum. The product was isolated as a pale yellow solid (1.44 g, 4.43 mmol, 65%). ^{1}H NMR (500 MHz, $CDCl_3$) ∂ / ppm: 8.72 (ddd, J = 4.9, 1.8, 0.9 Hz, 1H, H^{A6}), 8.57 (d, J = 8.0 Hz, 1H, H^{A3}), 8.51 (s, 1H, H^{B3}), 7.90 (td, J = 7.8, 1.8 Hz, 1H, H^{A4}), 7.64 (m, 4H, H^{C2+C3}), 7.41 (d, J = 1.7 Hz, 1H, H^{B5}), 7.38 (m, 1H, H^{A5}), 2.74 (s, 3H, H^{Me}). ^{13}C NMR (126 MHz, $CDCl_3$) ∂ / ppm: 158.8 (C^{B6}), 155.4 (C^{A2+B2}), 149.2 (C^{B4}), 148.8 (C^{A6}), 137.9 (C^{A4}), 137.1 (C^{C1}), 132.5 ($C^{C2/C3}$), 129.0 ($C^{C2/C3}$), 124.3 (C^{A5}), 124.0 (C^{C4}), 122.2 (C^{A3}), 121.6 (C^{B5}), 116.9 (C^{B3}), 24.6 (C^{Me}). IR (solid, ν, cm^{-1}): 3051 (w) 2911 (w) 1601 (m) 1580 (m) 1567 (m) 1544 (m) 1485 (m) 1449 (m) 1408 (m) 1378 (m) 1260 (w) 1214 (w) 1137 (w) 1104 (w) 1072 (m) 1043 (w) 1007 (m) 994 (m) 906 (w) 894 (w) 870 (w) 822 (s) 791 (s) 743 (m) 731 (m) 714 (w) 696 (m) 655 (m) 635 (w) 621 (m) 580 (w) 562 (w) 540 (w) 478 (s). MALDI-MS m/z: 325.0 $[M+H]^+$ (calc. 324.9), 246.4 $[M–Br+H]^+$ (calc. 246.1). UV-Vis (CH_2Cl_2, 1.00 × 10^{-5} mol dm^{-3}) λ_{max} nm (ε/ dm^3 mol^{-1} cm^{-1}): 249 (29950), 274 (25800), 310sh (9900). Calcd. for C_{17} H_{13} BrN_2 : C 62.79, H 4.03, N 8.61; found: C 62.51, H 4.17, N 8.76.

2.4 4-(4-Bromophenyl)-6,6'-dimethyl-2,2'-bipyridine

(*E*)-3-(4-Bromophenyl)-1-(6-methyl-2-pyridyl)-2-propen-1-one (2.00 g, 6.60 mmol) was dissolved in MeOH (90 ml) and 1-(2-oxopropyl)pyridinium chloride (1.14 g, 6.60 mmol) was added. The reaction mixture was treated with NH_4OAc (15.3 g, 198 mmol) and heated at reflux for 24 h. It was left to cool then placed in the refridgerator overnight. The precipitate that formed was collected by filtration, washed with H_2O (3 × 15 mL) and MeOH (3 × 15 mL), and dried overnight in a desiccator. The product was isolated as a pale brown solid (830 mg, 2.44 mmol, 37%). ^{1}H NMR (500 MHz, $CDCl_3$) δ/ppm: 8.46 (s, 1H, H^{B3}), 8.28 (d, J = 7.8 Hz, 1H, H^{A3}), 7.74 (t, J = 7.7 Hz, 1H, H^{A4}), 7.63 (m, 4H, H^{C2+C3}), 7.36 (d, J = 1.6 Hz, 1H, H^{B5}), 7.20 (d, J = 7.5 Hz, 1H, H^{A5}), 2.71 (s, 3H, H^{MeB}), 2.68 (s, 3H, H^{MeA}). ^{13}C NMR (126 MHz, $CDCl_3$) δ/ppm: 158.68 (C^{B2}), 158.11 (C^{A2}), 156,16 (C^{B6}), 155.13 (C^{A6}), 148.8 (C^{B4}), 137.7 (C^{A4}), 137.6 (C^{C1}), 132.2 ($C^{C2/C3}$), 129.0 ($C^{C2/C3}$), 123.8 (C^{A5}), 123.6 (C^{C4}), 121.1 (C^{B5}), 119.0 (C^{A3}), 116.7 (C^{B3}), 24.7 (C^{MeB}), 24.6 (C^{MeA}). IR: 2917 (w) 1607 126(w) 1573 (m) 1545 (m) 1490 (m) 1458 (w) 1415 (m) 1381 (m) 1366 (m) 1258 (m) 1209 (w) 1157 (w) 1104 (w) 1075 (w) 1008 (m) 913 (w) 898 (w) 861 (w) 823 (s) 801 (s) 782 (m) 745 (m) 715 (m) 683 (s) 646 (m) 589 (s) 573 (s) 552 (s) 534 (s) 517 (s) 479 (m). MALDI-MS m/z: 341.1 $[M+H]^+$ (calc: 340.0). UV-Vis (CH_2Cl_2, 1.00 × 10^{-5} mol dm^{-3}) λ_{max} nm (ε/ dm^3 mol^{-1} cm^{-1}) 249 (31900), 272 (24900), 309 sh (13800). Calcd. for $C_{18}H_{15}BrN_2$: C 63.73, H 4.46, N 8.26; found: C 63.59, H 4.64, N 8.61.

*2.5 Compound **2***

PPh_3 (5.56 g, 21.0 mmol) and $NiCl_2{\cdot}6H_2O$ (1.27 g, 5.36 mmol) were dissolved in DMF (28 ml) under an N_2 atmosphere. Zinc powder (346 mg, 5.36 mmol) was added and the

solution was left to stir for 1 h at 50 ^{o}C during which time it turned dark red. 4-(4-Bromophenyl)-6-methyl-2,2'-bipyridine (1.73 g, 5.36 mmol) was added and the mixture was stirred at 50 ^{o}C for 12 h. The reaction mixture was poured into aqueous NH_3 solution (200 mL, 10%) and extracted with CH_2Cl_2 (3 × 50 mL). The organic phase was washed with H_2O (3 × 50 mL), dried over $MgSO_4$ and overlayed with EtOH (200 mL). The CH_2Cl_2 was removed under reduced pressure and the EtOH phase was left in a freezer (–20 °C) for 2 h. A white crystalline solid formed and was collected by filtration, washed with cooled EtOH and dried in vacuo. Compound **2** was isolated as a white solid (770 mg, 1.57 mmol, 59%). MP: 240 ^{o}C. ^{1}H NMR (500 MHz, $CDCl_3$) ∂ / ppm: 8.72 (ddd, J = 4.8, 1.8, 0.9 Hz, 2H, H^{A6}), 8.53 (d, J= 1.6 Hz, 2H, H^{B3}), 8.50 (m, 2H, H^{A3}), 7.88 (m, 4H, $H^{C2/C3}$) overlapping with 7.84 (m, 2H, H^{A4}), 7.78 (m, 4H, H^{C3}), 7.47 (d, J = 1.6 Hz , 2H, H^{B5}), 7.34 (dd, J = 7.5, 4.8 Hz, 2H, H^{A5}), 2.74 (s, 6H, H^{Me}). ^{13}C NMR (126 MHz, $CDCl_3$) ∂ / ppm: 158.6 (C^{B6}), 156.3 (C^{A2}), 156.13 (C^{B2}), 149.2, (C^{C4}), 149.2 (C^{A6}), 141.0 (C^{B4}), 137.8 (C^{C1}), 137.2 (C^{A4}), 127.8 ($C^{C2/C3}$), 127.7 ($C^{C2/C3}$), 124.1 (C^{A5}), 121.9 (C^{A3}), 121.4 (C^{B5}), 116.4 (C^{B3}), 25.0 (C^{Me}). IR (solid, ν, cm^{-1}): 3056 (w) 2959 (w) 2918 (w) 1911 (w) 1600 (m) 1580 (s) 1564 (s) 1545 (m) 1507 (m) 1472 (m) 1448 (m) 1425 (m) 1407 (m) 1389 (s) 1344 (m) 1260 (m) 1217 (m) 1111 (m) 1088 (m) 1074 (m) 1039 (m) 1004 (m) 988 (m) 964 (m) 907 (m) 888 (m) 848 (m) 821 (s) 791 (s) 740 (s) 732 (s) 681 (m) 667 (m) 647 (m) 628 (m) 620 (s) 582 (m) 564 (m) 548 (m) 525 (m) 498 (m). UV-Vis (CH_2Cl_2, 1.00 × 10^{-5} mol dm^{-3}) λ_{max} nm (ε/ dm^3 mol^{-1} cm^{-1}): 306 (57400). Calcd. for $C_{34}H_{26}N_4$: C 83.24, H 5.34, N 11.42; found: C 83.49, H 5.43, N 11.54.

*2.6 Compound **3***

PPh_3 (6.19 g, 23.6 mmol) and $NiCl_2{\cdot}6H_2O$ (1.4 g, 5.90 mmol) were dissolved in DMF (30 mL) under N_2, and zinc powder (0.39 mg, 5.90 mmol) was added. After heating to 50 ^{o}C,

the mixture was stirred for 1 h during which time it turned red. 4-(4-Bromophenyl)-6,6'-dimethyl- 2,2'-bipyridine (2.00 g, 5.90 mmol) was added and the mixture was left stirring at 50 ^{o}C for 12 h. The reaction mixture was poured into aqueous NH_3 solution (200 mL, 10%), extracted with CH_2Cl_2 (3 × 50 mL). The solid retained in the organic phase was filtered, recrystallized from toluene and washed with toluene and EtOH. Compound **3** was isolated as colourless needles which were dried under vacuum (430 mg, 0.829 mmol, 28%). MP: 308 ^{o}C. ^{1}H NMR (500 MHz, MeCN) ∂ / ppm: 8.64 (s, 2H, H^{B3}), 8.42 (s, 2H, H^{A3}), 7.93 (m, 4H, H^{C2}) 7.84–7.76 (overlapping m, 6H, H^{A4+C3}), 7.52 (s, 2H, H^{B5}), 7.25 (d, 2H, H^{A5}) , 2.81 (s, 3H, H^{Me-B}), 2.73 (s, 3H, H^{Me-A}). ^{13}C NMR (126 MHz, $CDCl_3$) ∂ / ppm: 158.3 (C^{B6}), 158.1 (C^{A6}), 149.9 (C^{B4}), 141.3 (C^{C4}), 138.0 (C^{A4}), 137.4 (C^{C1}), 128.0 (C^{C2}), 127.9 (C^{C3}), 124.0 (C^{A5}), 121.5 (C^{B5}), 119.5 (C^{A3}), 117.4 (C^{B3}), 24.3 (C^{Me-A}), 24.1 (C^{Me-B}) (C^{A2} and C^{B2} not resolved). IR (solid, ν, cm^{-1}): 3673 (w) 2989 (w) 2915 (w) 1604 (m) 1583 (s) 1539 (s) 1506 (m) 1459 (m) 1431 (m) 1414 (m) 1390 (m) 1259 (w) 1218 (w) 1158 (w) 1117 (w) 1074 (m) 1033 (m) 1005 (m) 896 (m) 874 (m) 859 (m) 850 (m) 848 (m) 829 (m) 820 (m) 805 (s) 779 (m) 750. (m) 661 (m) 625 (s) 593 (w) 571 (w) 554 (m) 536 (m) 527 (m) 515 (m) 500 (m). UV-Vis (CH_2Cl_2, 1.00 × 10^{-5} mol dm^{-3}) λ_{max} / nm (ε/ dm^3 mol^{-1} cm^{-1}) 304 (71000). Calcd. for $C_{36}H_{30}N_4$: C 83.37, H 5.83, N 10.80; found: C 83.53, H 5.92, N 10.81.

*2.7 [Ru(bpy)$_2$(**2**)][PF$_6$]$_2$*

cis-[$Ru(bpy)_2Cl_2$] (200 mg, 0.413 mmol) and **2** (200 mg, 0.408 mmol) were suspended in EtOH (15 mL) in a microwave vial and heated at 120 ^{o}C in a microwave reactor for 1.5 h. After cooling to room temperature, an excess of solid NH_4PF_6 was added and the mixture was left to stir for 20 min. The orange precipitate that formed was collected by filtration, washed with water, EtOH and Et_2O (20 mL of each). The solid was dissolved in MeCN,

dried over $MgSO_4$ and the solvent then removed under reduced pressure. The crude product was purified by column chromatography (neutral alumina, MeCN/saturated aqueous KNO_3/H_2O, 17 : 1 : 0.5) and the first two fractions were collected and combined. An excess of aqueous NH_4PF_6 was added, the mixture filtered and the solid residue washed with water, EtOH and Et_2O (20 mL of each). The product was purified again (basic alumina, toluene/MeCN, 3:2). The first fraction was collected, solvent removed under reduced pressure to yield $[Ru(bpy)_2(\mathbf{2})][PF_6]_2$ as an orange solid (110 mg, 0.122 mmol, 29%). ^{1}H NMR (500 MHz, CD_2Cl_2) δ/ppm: 8.67 (ddd, J = 4.7, 1.9, 0.9 Hz, 1H, H^{A6}), 8.62 (d, J = 8.3 Hz, 1H, $H^{F3/G3/H3/I3/J3}$), 8.58 (d, J = 2.2 Hz, 1H, $H^{E3/B3}$), 8.54 (d, J = 1.6 Hz, 1H, $H^{E3/B3}$), 8.53–8.46 (m, 3H, $H^{A3 + two\ of\ F3/G3/H3/I3/J3}$), 8.46–8.38 (m, J = 10.5, 8.1, 1.0 Hz, 2H, $H^{two\ of\ F3/G3/H3/I3/J3}$), 8.16–8.05 (m, 4H, $H^{F6 + three\ of\ F4/G4/H4/I4/J4}$), 8.02 (td, J = 7.9, 1.5 Hz, 1H, $H^{F4/G4/H4/I4/J4}$), 8.00–7.93 (m, 3H, $H^{F4/G4/H4/I4/J4 + D2/C3}$), 7.91–7.83 (m, 5H, $H^{A4 + C2/D3 + D2/C3}$), 7.81 (d, J = 8.5 Hz, 2H, $H^{C2/D3}$), 7.73 (dd, J = 5.7, 1.3 Hz, 1H, $H^{G6/H6/I6/J6}$), 7.65 (m, 2H, $H^{G6/H6/I6/J6 + B5/E5}$), 7.54 (m, 2H, $H^{F5/G5/H5/I5/J5 + G6/H6/I6/J6}$), 7.51–7.44 (m, 3H, $H^{B5/E5 + F5/G5/H5/I5/J5 + G6/H6/I6/J6}$), 7.47 (m, 4H, $H^{A5 + three\ of\ F5/G5/H5/I5/J5}$), 2.69 (s, 3H, $H^{Me\text{-}B}$), 1.97 (s, 3H, $H^{Me\text{-}E}$). ^{13}C NMR (126 MHz, CD_2Cl_2) ∂ / ppm: 165.5 ($C^{E6/B6}$), 159.1 ($C^{B6/E6}$), 158.7 ($C^{A2/B2/E2/F2/G2/H2/I2/J2}$), 157.9 ($C^{A2/B2/E2/F2/G2/H2/I2/J2}$), 157.5 ($C^{A2/B2/E2/F2/G2/H2/I2/J2}$), 157.4 ($C^{A2/B2/E2/F2/G2/H2/I2/J2}$), 157.3 ($C^{A2/B2/E2/F2/G2/H2/I2/J2}$), 157.0 ($C^{A2/B2/E2/F2/G2/H2/I2/J2}$), 156.4 ($C^{A2/B2/E2/F2/G2/H2/I2/J2}$), 156.3 ($C^{A2/B2/E2/F2/G2/H2/I2/J2}$), 153.0 ($C^{F6}$), 151.7 ($C^{G6/H6/I6/J6}$) 151.5 ($2C^{two\ of\ G6/H6/I6/J6}$), 151.4 ($C^{G6/H6/I6/J6}$), 150.3 ($C^{B4/E4}$), 149.5 ($C^{A6)}$, 149.2 ($C^{B4/E4}$), 143.0 ($C^{C1/D4}$), 140.7 ($C^{C1/D4}$), 139.0 ($C^{F4/G4/H4/I4/J4}$), 138.7 ($2C^{two\ of\ F4/G4/H4/I4/J4}$), 138.6 ($C^{C4/D1}$), 138.5 ($C^{F4/G4/H4/I4/J4}$), 138.3 ($C^{F4/G4/H4/I4/J4}$), 137.6 ($C^{A4}$), 134.8 ($C^{C4/D1}$), 128.9 ($C^{F5/G5/H5/I5/J5}$), 128.7 ($C^{F5/G5/H5/I5/J5}$), 128.5 ($C^{C2/C3/D2/D3 + F5/G5/H5/I5/J5}$), 128.4 ($C^{A5}$), 128.3 ($C^{C2/C3/D2/D3}$), 128.2 ($C^{C2/C3/D2/D3}$), 128.15 ($C^{C2/C3/D2/D3}$), 128.1 ($C^{F5/G5/H5/I5/J5}$), 126.5 ($C^{B5/E5}$), 125.4 ($C^{F3/G3/H3/I3/J3}$), 125.1 ($C^{F3/G3/H3/I3/J3}$), 125.0

($C^{F3/G3/H3/I3/J3}$), 124.9 ($C^{F3/G3/H3/I3/J3}$), 124.8 ($C^{F3/G3/H3/I3/J3}$), 124.4 ($C^{F5/G5/H5/I5/J5}$), 121.7 (C^{A3}), 121.5 ($C^{B5/E5}$), 120.0 ($C^{B3/E3}$), 116.3 ($C^{B3/E3}$), 26.7 (C^{Me-E}), 24.9 (C^{Me-B}). IR (solid, ν, cm^{-1}): 3664 (w) 2919 (w) 1671 (w) 1603 (m) 1584 (m) 1566 (w) 1505 (w) 1462 (m) 1446 (m) 1392 (m) 1241 (m) 1162 (m) 1066 (m) 1003 (m) 827 (s) 761 (s) 730 (s) 682 (m) 620 (m) 555 (s). ESI-MS m/z: 452.1 $[M–2PF_6]^{2+}$ (calc: 452.1). UV-Vis (MeCN, 1.00 × 10^{-5} mol dm^{-3}) λ_{max} / nm (ε/ dm^3 mol^{-1} cm^{-1}) 245 (35900), 289 (860000), 254 sh (31600), 331 sh (43800), 424 sh (13400), 453 (17000). Calc. for $C_{54}H_{42}F_{12}N_8P_2Ru{\cdot}H_2O$ C 53.51, H 3.66, N 9.25; found: C 53.48, H 4.14, N 9.12.

2.9 Crystallography

Single crystal data were collected on a Bruker APEX-II diffractometer with data reduction, solution and refinement using the programs APEX [37] and SHELX-13 [38]. The structural diagrams and structure analysis were carried out using Mercury v. 3.0.1 or 3.3 [39,40].

2: $C_{34}H_{26}N_4$, M = 490.59, colourless needle, triclinic, space group P–1, a = 8.9001(9), b = 10.1205(11), c = 14.4840(18) Å, α = 78.320(6), β = 82.262(6), γ = 89.959(6)°, U = 1265.5(2) $Å^3$, Z = 2, D_c = 1.287 Mg m^{-3}, μ(Mo-Kα) = 0.077 mm^{-1}, T = 123 K. Total 16929 reflections, 5037 unique, R_{int} = 0.0504. Refinement of 3057 reflections (345 parameters) with $I > 2\sigma(I)$ converged at final $R1$ = 0.0498 ($R1$ all data = 0.0990), $wR2$ = 0.1114 ($wR2$ all data = 0.1319), gof = 0.997.

Crystallographic data have been deposited with the CCDC (Cambridge Crystallographic Data Centre, 12 Union Road, Cambridge CB2 1EZ, UK; fax +44 1223 336 033; e-mail: deposit@ccdc.cam.ac.uk or www: http://www.ccdc.cam.ac.uk) and may be obtained free of charge on quoting the deposition numbers CCDC 1032042.

2.10 DSSC fabrication

DSSCs were prepared using a similar procedure to that described by Grätzel and coworkers [41,42]. Solaronix Test Cell Titania Electrodes were used for the photoanodes. These electrodes were washed with EtOH, then sintered at 450 ^{o}C for 30 min, cooled to ≈80 ^{o}C, and then dipped into a DMSO solution of ligand **4** (1 mM) for 1 day (24 h). The electrode was removed from the solution, washed with DMSO and EtOH and dried with a heat gun (60 °C). The electrode was then soaked in a MeCN solution of $[Cu(MeCN)_4][PF_6]$ (2 mM) for 24 h, removed from the solution and rinsed with MeCN. Finally, it was immersed in a CH_2Cl_2 solution (1 mM) of ligand **1**, **2** or **3** or a MeCN solution of $[Ru(bpy)_2(\mathbf{2})][PF_6]_2$ for 24 h, removed and rinsed with CH_2Cl_2 or MeCN. For multi-generation dyes (see text), the $[Cu(MeCN)_4][PF_6]$/ancillary ligand dipping steps were repeated 2 or 3 times. Solaronix Test Cell Platinum Electrodes were used for the photocathodes, and volatile organic impurities were removed by heating for 30 min at 450 ^{o}C.

The dye-covered TiO_2 electrode and Pt counter electrode were assembled using thermoplast hot-melt sealing foil (Solaronix Test Cell Gaskets) by heating while pressing them together. The electrolyte was introduced into the DSSC by vacuum backfilling; the electrolyte composition was LiI (0.1 M), I_2 (0.05 M), 1-methylbenzimidazole (0.5 M) and 1-butyl-3-methylimidazolinium iodide (0.6 M) in 3-methoxypropionitrile. The hole in the counter electrode was sealed using hot-melt sealing foil (Solaronix Test Cell Sealings) and a cover glass (Solaronix Test Cell Caps).

2.11 DSSC and external quantum efficiency (EQE) measurements

The solar cell measurements and testing protocol were performed using fully masked cells. A black coloured copper sheet was used for masking with a single aperture of average area 0.06012 cm^2 (standard deviation of 1%) placed over the dye-sensitized TiO_2 circle. The area of the aperture in the mask was smaller than the active area of the TiO_2 (0.36 cm^2). For complete masking, tape was also applied over the edges and rear of the cell. Measurements were made by irradiating the DSSC from behind using a SolarSim 150 instrument (100 mW cm^{-2} = 1 sun), and the simulated light power was calibrated by using a silicon reference cell.

The external quantum efficiency (EQE) measurements were performed on a Spe-Quest quantum efficiency setup from Rera Systems (Netherlands) equipped with a 100 W halogen lamp (QTH) and a lambda 300 grating monochromator from Lot Oriel. The monochromatic light was modulated to 3Hz using a chopper wheel from ThorLabs. The cell response was amplified with a large dynamic range IV converter from CVI Melles Griot and then measured with a SR830 DSP Lock-In amplifier from Stanford Research.

2.12 Scanning electrochemical microscopy (SECM)

SECM experiments were carried out using a Uniscan M370 SECM operating in feedback mode coupled to a three electrode cell consisting of a Uniscan 15 μm Pt working ultramicroelectrode (UME) close to the substrate surface, a Pt counter and printed Ag/AgCl reference electrodes. The experiments were performed over FTO with a copper(I) dye-sensitized TiO_2 layer. UME tips were acid cycled [43] polished and checked under an optical microscope before use. Before the SECM measurements, the substrate surface was levelled using a Wyler high precision (type 72) circular spirit level and checked by measuring line scans for tilt in both the X and Y directions. The electrolyte comprised tetracyanoquinodimethane (TCNQ) and tetrabutylammonium

hexafluoridophosphate ($TBAPF_6$) in 3-methoxypropionitrile. For retraction curve measurements the concentrations of TCNQ and $TBAPF_6$ were 1 mM and 0.02 M, respectively. For area scans, more dilute concentrations of 0.33 mM and 6.67 mM respectively were used. Approach curves were run at appropriate potentials, in small increments (2 μm every 5 s) in the dark, until the current reached 50% of the bulk current.

For measurements under illumination, a modified SECM cell in which a controlled light source irradiates part of the dye-functionalized surface was constructed as previously detailed [44]. A Thorlabs OSL1-EC halogen lamp source was coupled to Thorlabs BFH48-1000 optical wiring (Ø1 mm core) using an SMA adaptor. This was placed through a hole (1.1 mm diameter) in the base of the SECM cell and a piece of Laseroptik UV-FS glass (refractive index Na = 0.48, thickness = 6.35 mm, transmission range 200-2100 nm) was placed above it in a custom made Teflon base contained in a standard SECM μ-holder. Calibration at different light intensities was carried out using a Thorlabs PM100 power meter fitted with a Thorlabs model D3MM detector head, to measure the total light striking the surface. From this, the light intensity (per cm^2) was determined and calibrated relative to the amount of light emitted from the source lamp at different settings.

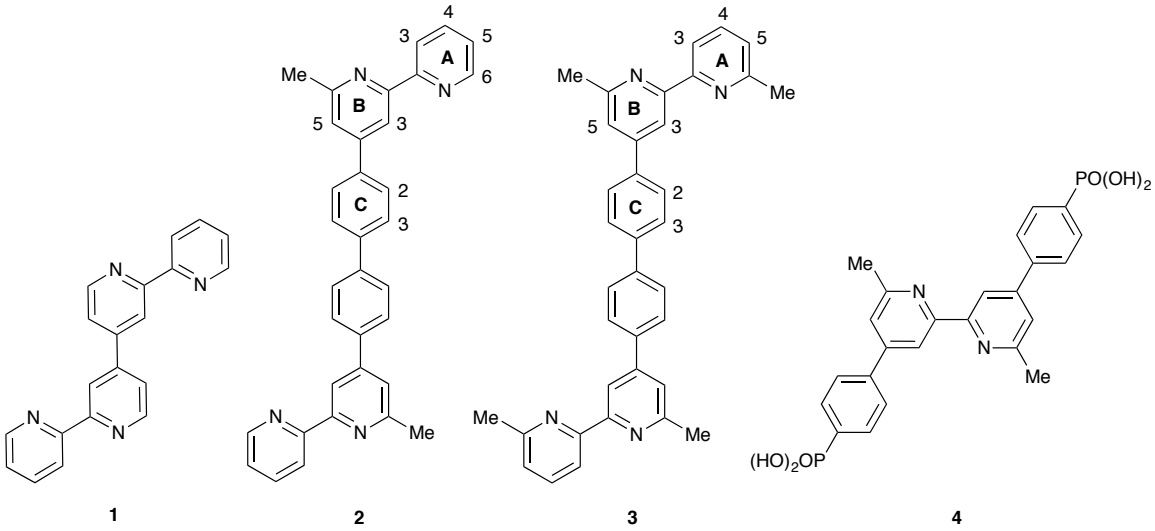

Scheme 3. Structures of ligands with atom numbering for NMR assignments for **2** and **3**.

3 Results and discussion

3.1 Ligand syntheses and characterisations

The choice of ligands **1**–**3** as ancillary ligands in $[Cu(L_{anchor})(L_{ancillary})]^+$ dyes has two goals. Firstly, in a bis(diimine) complex, copper(I) is stabilized against oxidation by using substituents such as methyl in the 6,6'-positions [45]. Anchoring ligand **4** (Scheme 3) is a 6,6'-dimethyl derivative, and we were interested in establishing whether it was also necessary for the ancillary ligand to contain such substituents. We have previously demonstrated that the efficiency of a $[Cu(\mathbf{4})(L_{ancillary})]^+$ dye is strongly affected by the nature of the 6,6'-substituents in $L_{ancillary}$ [25], but have not investigated $[Cu(\mathbf{4})(L_{ancillary})]^+$ dyes in which the ancillary ligand does not bear substituents at the 6,6'-positions. The second reason for selecting ligands **1**–**3** is that each contains two metal-binding domains and can potentially form surface-bound copper(I) complexes that can function as ligands, i.e. an extension of the 'complexes-as-ligands' approach [19,20] to 'surfaces-as-ligands'.

The strategy chosen for the preparation of ligands **1**–**3** (Scheme 3) was based on the nickel(0)-catalysed coupling of 4-chloro-2,2'-bipyridine reported for **1** [36]. However, we found it convenient to adapt the procedure using the method of Tiecco and Testaferri [46]. Ligands **1**, **2** and **3** were isolated in 19, 59 and 28% yields, respectively. To the best of our knowledge, compounds **2** and **3** have not previously been reported. The ^{1}H and ^{13}C NMR spectra were assigned using COSY, NOESY, HMQC and HMBC methods and Figure 2 shows the aromatic region of the ^{1}H NMR spectrum of **2**, confirming the substitution pattern in the bpy domain. On going from **2** to **3**, the presence of the signal at ∂ 8.72 ppm in the spectrum of **2** but not in **3** is consistent with the introduction of the

methyl group. In agreement with this is the appearance of a singlet at ∂ 2.74 ppm for the methyl group in **2**, and two singlets (∂ 2.81 and 2.73 ppm) in the spectrum of **3** for the 6- and 6'-methyl substituents. Arene protons H^{C2} and H^{C3} were distinguished by the appearance of NOESY cross peaks between H^{C2}/H^{B3} and H^{C2}/H^{B5}.

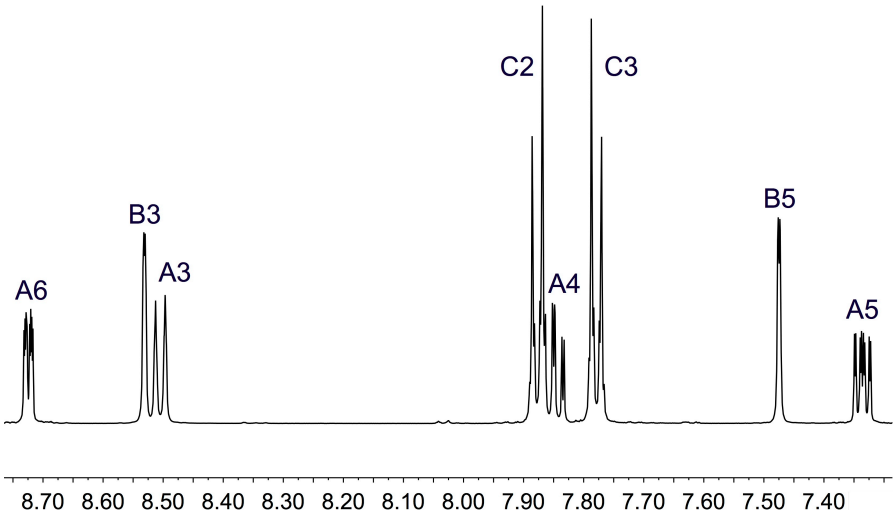

Figure 2. Aromatic region of the 500 MHz ^{1}H NMR spectrum of **2** ($CDCl_3$, 295 K). See Scheme 3 for atom labelling.

The structure of **2** was confirmed by a single-crystal structure determination. Crystals were grown from a CH_2Cl_2 solution overlaid with hexanes. Compound **2** crystallizes in the triclinic space group *P*–1 and the molecular structure is shown in Figure 3. Alleviation of repulsions between the *ortho*-hydrogen atoms of adjacent rings leads to **2** having a twisted conformation (angles between the planes of the rings containing N1/N2, N2/C12, C12/C21, C21/N3 and N3/N4 = 8.1, 23.8, 34.6, 18.5, 1.8^o, respectively. In the solid state, individual molecules are rendered chiral by this twisting and pairs of enantiomers engage in an embrace, packing along the *b*-axis (Figure 4). Between each centrosymmetric pair of molecules, the arene rings containing C18 and C18i (symmetry code i = 1–*x*, –*y*, 1–*z*) lie over each other, but the π-stacking interaction

is only weak; the separation of the ring planes = 3.82 Å and inter-centroid distance = 4.34 Å.

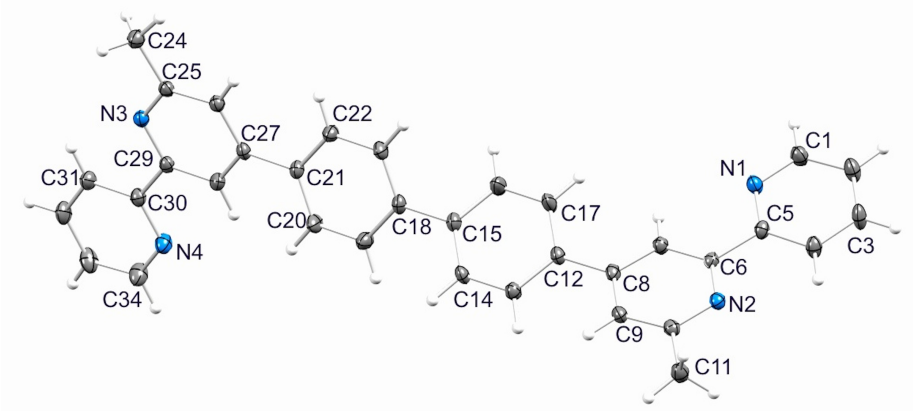

Figure 3. Molecular structure of **2** (ellipsoids plotted at 40% probability level). Selected bond lengths: N1–C1 = 1.333(2), N1–C5 = 1.340(2), N2–C6 = 1.344(2), N2–C10 = 1.345(2), C25–N3 = 1.339(2), C29–N3 = 1.342(2), C30–N4 = 1.337(2), C34–N4 = 1.338(3), C10–C11 = 1.495(3), C24–C25 = 1.496(3) Å. (Colour online)

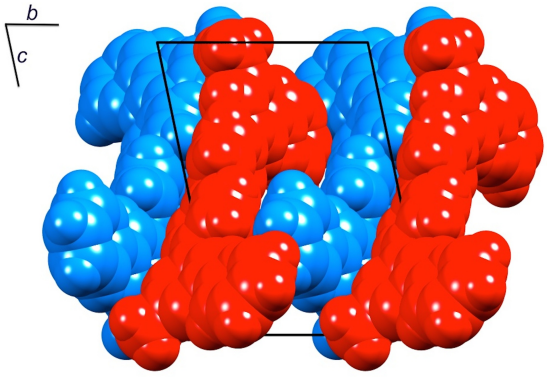

Figure 4. Packing of centrosymmetric pairs of molecules of **2**; red and blue coloured molecules have opposite chirality. (Colour online)

The solution absorption spectra of componds **1**–**3** are compared in Figure 5. The intense absorptions arise from π*←π and π*←n transitions, and the increase in absorption intensity on going from **1** to **2** and **3** is consistent with the introduction of the biphenyl spacer and consequent extension of π-conjugation.

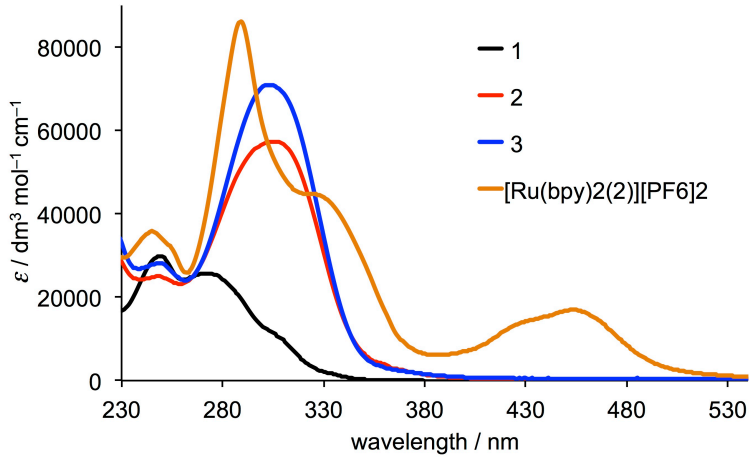

Figure 5. Solution absorption spectra of **1**–**3** (CH_2Cl_2, 1.00×10^{-5} mol dm^{-3}) and of $[Ru(bpy)_2(\mathbf{2})][PF_6]_2$ (MeCN, 1.00×10^{-5} mol dm^{-3}).

*3.2 DSSC assembly and performances for $[Cu(\mathbf{4})(L_{ancillary})]^+$ with $L_{ancillary}$ = **1**, **2** or **3***

We initially investigated the performances of DSSCs containing surface-bound heteroleptic copper(I) dyes $[Cu(\mathbf{4})(L_{ancillary})]^+$ with $L_{ancillary}$ = **1**, **2** or **3**. FTO/TiO_2 was first functionalized with the phosphonic acid **4** (Scheme 3) by immersing the electrode in a DMSO solution of **4**. After drying the electrode, it was soaked in a MeCN solution of $[Cu(MeCN)_4][PF_6]$, before finally being immersed in a CH_2Cl_2 solution of either **1**, **2** or **3**. After washing with CH_2Cl_2 and drying, the electrode retained an orange colour. The stepwise assembly is summarized in Scheme 4.

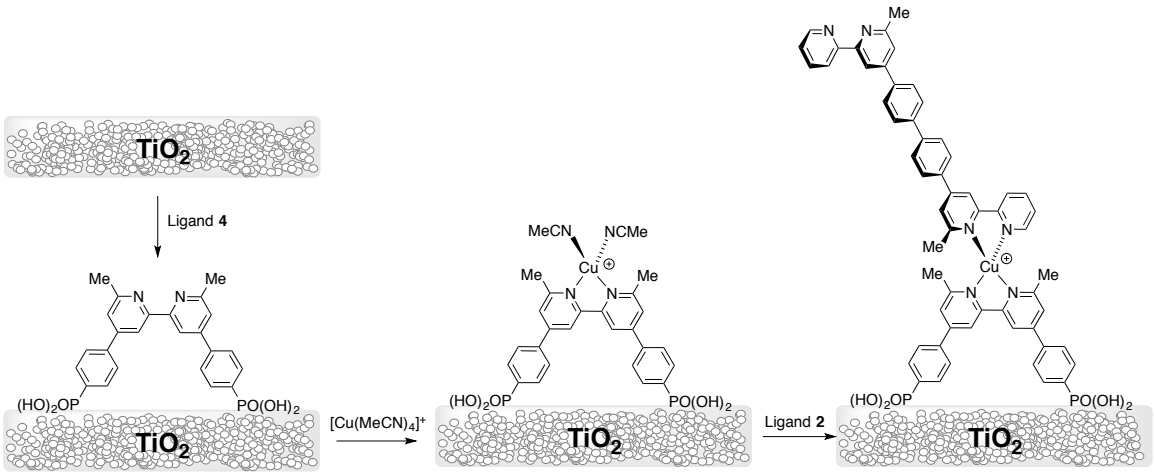

Scheme 4. Stepwise assembly of a copper(I) dye exemplified by formation of surface-bound $[Cu(\mathbf{4})(\mathbf{2})]^+$.

The DSSC performance parameters measured on the day of cell fabrication are given in Table 1. Duplicate cells were made and the best data for each pair of cells are given in the table; with the exception of the cell containing $[Cu(\mathbf{4})(\mathbf{1})]^+$, both cells of each pair performed similarly within experimental error. Fill factors (*ff*) for all DSSCs including the N719 reference cell are in the range 71–74%. When measuring with respect to a DSSC containing N719, it is convenient to give relative values of photon-to-current efficiency, setting η for N719 to 100% (Table 1). This allows direct comparison of sets of data from different experiments or different solar simulators [47]. The introduction of the 6-methyl substituent on going from $[Cu(\mathbf{4})(\mathbf{1})]^+$ to $[Cu(\mathbf{4})(\mathbf{2})]^+$ improves both the short-circuit current density (J_{SC}) and the open-circuit voltage (V_{OC}), and the same trend is observed on going from $[Cu(\mathbf{4})(\mathbf{2})]^+$ to $[Cu(\mathbf{4})(\mathbf{3})]^+$ as is seen in the *J–V* curves in Figure 6. The global efficiency of the DSSC improves from 1.16 to 1.69 to 2.16% as one and then two methyl substituents are introduced. Figure 7 shows the EQE spectra for the DSSCs, recorded on the day the cells were prepared. All show λ_{max} values of 480 nm, and

EQE_{max} is enhanced from 24.7% for $[Cu(\mathbf{4})(\mathbf{1})]^+$ to 30.4% for $[Cu(\mathbf{4})(\mathbf{1})]^+$ to 34.0% for $[Cu(\mathbf{4})(\mathbf{3})]^+$.

Table 1 Performances of masked DSSCs using the dyes $[Cu(\mathbf{4})(L_{ancillary})]^+$ ($L_{ancillary}$ = **1**–**3**).

Dye	J_{SC} / mA cm^{-2}	V_{OC} / mV	*ff* / %	η / %	Relative η / %
$[Cu(\mathbf{4})(\mathbf{1})]^+$	3.13	524	70.9	1.16	16.2
$[Cu(\mathbf{4})(\mathbf{2})]^+$	4.18	548	73.7	1.69	23.6
$[Cu(\mathbf{4})(\mathbf{3})]^+$	5.20	566	73.3	2.16	30.1
N719	15.7	628	72.9	7.17	100

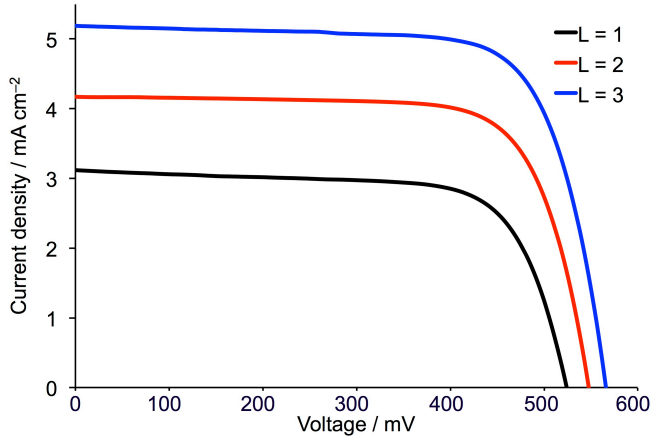

Figure 6. J–V curves for DSSCs containing the dyes $[Cu(\mathbf{4})(L_{ancillary})]^+$ ($L_{ancillary}$ = **1**–**3**).

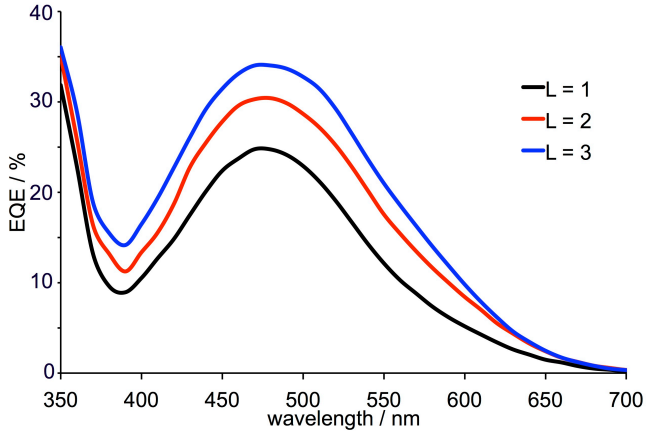

Figure 7. EQE curves for DSSCs containing the dyes $[Cu(\mathbf{4})(L_{ancillary})]^+$ ($L_{ancillary}$ = **1**–**3**).

3.3 Dyes with second and third generation copper(I) domains

Each of the anchored dyes $[Cu(\mathbf{4})(L_{ancillary})]^+$ ($L_{ancillary}$ = **1**–**3**) contains a peripheral bpy domain capable of binding a second copper(I) centre. Since the results of the first experiments confirmed the importance of retaining the 6,6'-dimethyl substitution pattern in the ancillary ligand, we focused on modifying $[Cu(\mathbf{4})(\mathbf{3})]^+$ in a 'complexes-as-ligands' approach. Dye modification was aimed at increasing the separation between the site of electron injection (anchoring ligand) and hole-transfer domain (periphery of the dye). Each FTO/TiO_2 electrode was dipped sequentially into a DMSO solution of **4**, a MeCN solution of $[Cu(MeCN)_4][PF_6]$, and a CH_2Cl_2 solution of **3**. This corresponds to one dipping regime giving anchored dye $[(\mathbf{4})Cu(\mathbf{3})]^+$. Additional soaking cycles in $[Cu(MeCN)_4][PF_6]$ followed by **3**, gave $[(\mathbf{4})\{Cu(\mathbf{3})\}_2]^{2+}$ and $[(\mathbf{4})\{Cu(\mathbf{3})\}_3]^{3+}$, respectively (Scheme 5). After washing and drying, the orange colour of the functionalized TiO_2 persisted. MALDI-TOF mass spectrometry was used to evaluate the surface species adsorbed on an FTO/TiO_2 electrode that had undergone three dipping regimes. The functionalized TiO_2 was scratched off and the highest mass peak in the MALDI-TOF (m/z 1100.7) was assigned to $[Cu(\mathbf{3})_2]^+$ (calc. m/z 1099.4); the envelope showed a characteristic isotope pattern for Cu. A lower mass peak envelope at m/z 581.4 was assigned to $[Cu(\mathbf{3})]^+$; the separation of the peaks in the envelope was consistent with a singly charged ion. The observation of the ion $[Cu(\mathbf{3})_2]^+$ is direct evidence for the presence of surface-bound multinuclear species, subject to the proviso that major redistribution of ligands at copper(I) centres does not occur in the course of the laser irradiation. Attempts to use solid state absorption spectroscopy to quantify the presence of the extended conjugated systems were inconclusive. Each functionalized electrode giving an intense, ligand-centred absorption with λ_{max} = 360 nm, and a broad MLCT

band centred at ≈470 nm, but there was little variation in the absorbance on going from first to second to third generation dye, although solid state absorption spectroscopy of these systems is notoriously difficult to quantify due to the nanoparticulate and non-homogeneous nature of the substrates.

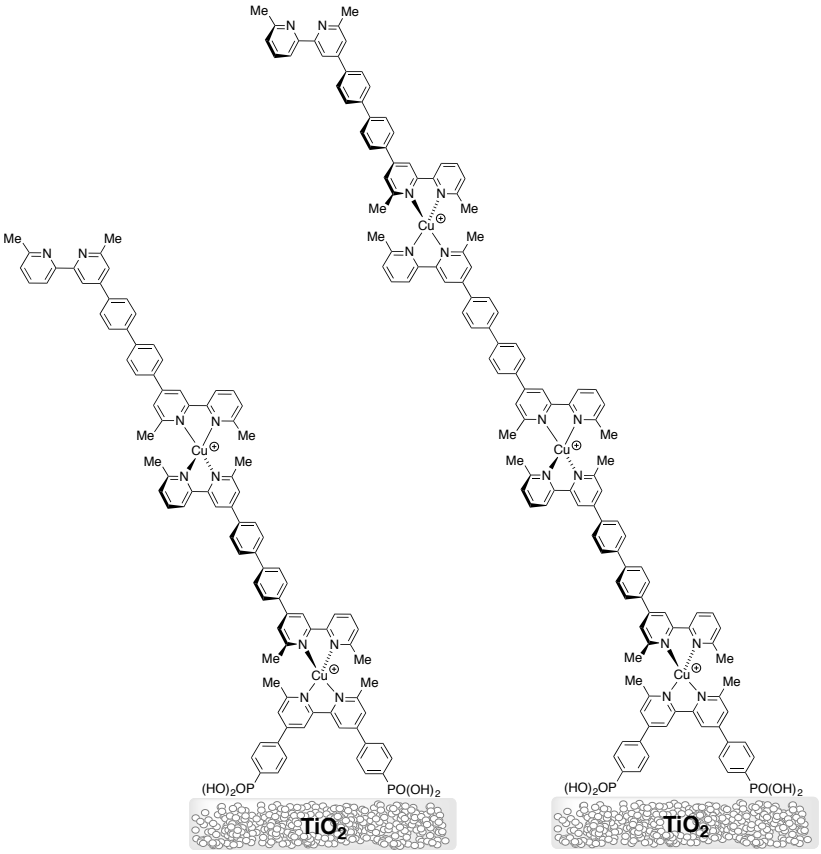

Scheme 5. Schematic representations of second and third generation surface-bound dyes $[(\mathbf{4})\{Cu(\mathbf{3})\}_2]^{2+}$ and $[(\mathbf{4})\{Cu(\mathbf{3})\}_3]^{3+}$ as generated through multiple sequential dipping cycles.

We therefore considered the technique of scanning electrochemical microscopy (SECM) for gaining information about the dye/electrolyte interface as an indirect probe for the changes in the surface rest charge state and hence the nuclearity of the surface-bound species (or strictly, the number of charged copper(I) centres present). We have

recently been developing SECM as a powerful method for analysing surface charge effects and investigating the interactions between excited state copper(I) dyes and the electrolyte [44]. In order to systematically compare the charge generated at the TiO_2 surface for the three generations of dye, each was examined using an electrolyte solution containing TCNQ. This was chosen as the active electrolyte for both its charge-carrying ability, (allowing for the detection of small charges at the surface even at low electrode potential), and its low chemical reactivity which reduces dissipation of charge, leading to longer lived species at the TiO_2 surface. SECM area scans of $[(\mathbf{4})\{Cu(\mathbf{3})\}_n]^{n+}$ (n = 1, 2 or 3) dye-sensitized FTO/TiO_2 electrodes were performed in the dark and under illumination (light intensity = 70 mW cm^{-2}). Irrespective of the number dipping cycles, an enhanced SECM response was observed when the electrode was illuminated compared to that measured in the dark. This conclusively demonstrates both the presence of dye on the surface and its ability to inject electrons into the semiconductor, but does not directly distinguish between the first, second or third generation complexes. Retraction scans were then conducted by initially placing the UME tip at a distance of ≈3–5 μm above the dye-functionalized TiO_2 surface and then slowly retracting it to a maximum distance from the surface of ≈1 mm. Retraction scans were recorded in the dark (Figure 8a) and under illumination (Figure 8b) and the curves demonstrate that the UME response increases along the series third > second > first generation dye. The retraction curves in Figure 8a indicate an increase with the number of dipping regimes leads to a larger response as the UME moves away from the surface. This is consistent with a greater number of copper charge centres on the TiO_2 surface, assumed to be a result of the generation of multinuclear surface-bound species. This analysis assumes that metal-binding capacity of the (fixed number of) **4** anchoring ligands on the surface is saturated with copper(I) in the first copper(I) dipping cycle. All of our previous studies indicate

that the optimized dipping procedures adopted ensure saturation of the anchoring ligands. The retraction curves measured under illumination (Figure 8b) indicate that more Cu^{+} ions are available for oxidation leading to an increase in current in the order third > second > first generation dye. The data support an increase in the number of {Cu(**3**)} units per adsorbed dye molecule.

Preliminary investigations of DSSCs made using one, two or three dipping cycles showed a small gain in the open-circuit voltage (566 to 588 mV) but a significant drop in the short-circuit current density (5.20 to 2.69 mA cm^{-2}) leading to poorer overall efficiencies. This may be due to aggregation of the rod-shaped dyes leading to quenching of the excited state [48]. These results parallel those of Kroeze, Durrant and coworkers [49] who observed that although increasing the length of alkyl chain-substituents on ruthenium(II)-based dyes results in slower charge recombination dynamics, this beneficial effect is offset by reduced rates of both electron injection and dye regeneration.

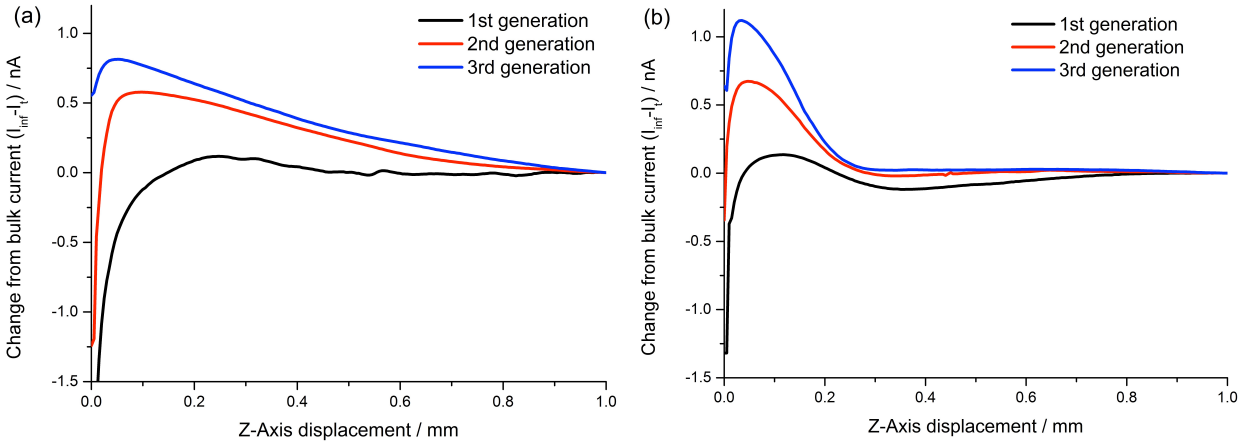

Figure 8. SECM retraction curves of sensitized electrodes (a) in the dark and (b) under illumination (70 mW cm^{-2}), with first, second and third generation dyes. The electrolyte contained TCNQ and $TBAPF_6$ in 3-methoxypropionitrile.

3.4 Using the 'surfaces-as-ligands' approach to assemble a heterometallic dye

The peripheral metal-binding domain in $[Cu(\mathbf{4})(L)]^+$ (L = **1**, **2** or **3**) can be utilized for assembly of heterometallic surface-bound complexes. For proof-of-principle studies, we chose to introduce a simple $\{Ru^{II}(bpy)_2\}$ unit. The combined coordination requirements of tetrahedral copper(I) and octahedral ruthenium(II) coupled with the DSSC performance trends in Table 1 led to a choice of **2** as the ligand bridging the two metal centres. The optimal ligand would be one with orthogonal copper(I) and ruthenium(II) metal-binding domains with 6,6'-dimethyl and no substitution at the 6,6'-positions, respectively. Ligand **2** was selected as a synthetically readily accessible compromise in which the single methyl substituent partially stabilizes the copper(I) centre, but does not significantly destabilize the ruthenium(II) centre. The synthetic approach adopted was the synthesis of $[Ru(bpy)_2(\mathbf{2})][PF_6]_2$ as a metalloligand followed by the use of $[Ru(bpy)_2(\mathbf{2})]^{2+}$ as an ancillary ligand for surface-bound complex assembly.

The reaction of **2** with *cis*-$[Ru(bpy)_2Cl_2]$ in ethanol under microwave conditions resulted, after workup, in the formation of $[Ru(bpy)_2(\mathbf{2})][PF_6]_2$ as a red solid in 29% yield. The electrospray mass spectrum exhibited a peak envelope at m/z 452.1 arising from the $[M–2PF_6]^{2+}$ ion. The ^1H and ^{13}C NMR spectra were assigned by 2D methods, starting with the signal at ∂ 8.67 ppm assigned to H^{A6} (see Scheme 6a). This proton is distinct from the remaining five bpy H^6 protons which are shifted to lower frequency because each lies over the π-system of an adjacent pyridine ring in the coordination sphere of the Ru^{2+} ion; these data are consistent with only one of the 6-methyl-2,2'-bipyridine units being bound to ruthenium. Further confirmation comes from the observation of two methyl signals at ∂ 2.69 and 1.97 ppm in the ^1H NMR spectrum and ∂ 26.7 and 24.9 ppm in the ^{13}C NMR spectrum. In free ligand **2**, the Me group gives rise to ^1H and ^{13}C NMR signals at ∂ 2.74 and 25.0 ppm, respectively. Proton H^{F6} in

$[Ru(bpy)_2(\mathbf{2})][PF_6]_2$ was assigned on basis of COSY and NOESY spectra, but overlap of signals (Figure 9) precluded differentiation between groups of pyridine H^3, H^4, H^5 or H^6 protons of the two unsubstituted bpy ligands. The solution absorption spectrum of $[Ru(bpy)_2(\mathbf{2})][PF_6]_2$ (Figure 5) exhibits the anticipated MLCT band (λ_{max} = 453 nm) which considerably extends the absorption of the ancillary ligand $[Ru(bpy)_2(\mathbf{2})]^{2+}$ to lower energies compared to **2** (Figure 5).

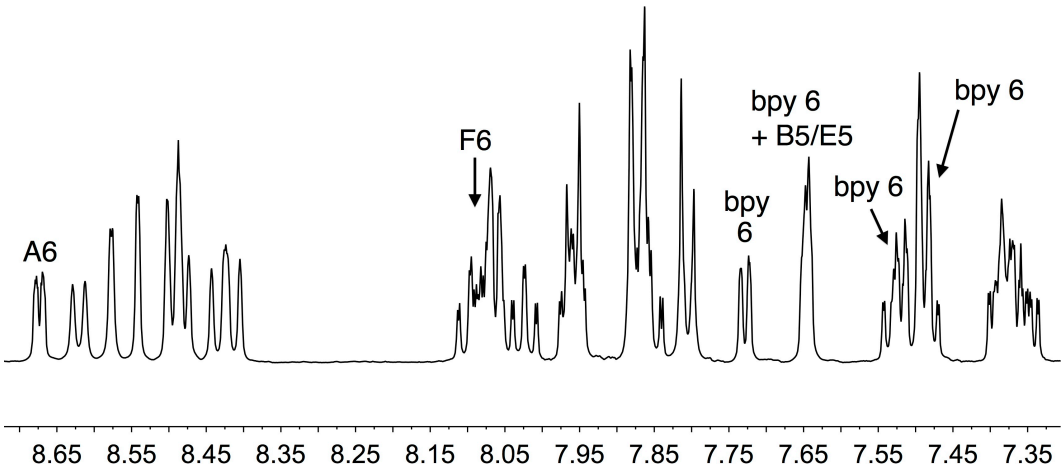

Figure 9. Aromatic region of the 500 MHz ^{1}H NMR spectrum of $[Ru(bpy)_2(\mathbf{2})][PF_6]$ (MeCN, 295 K).

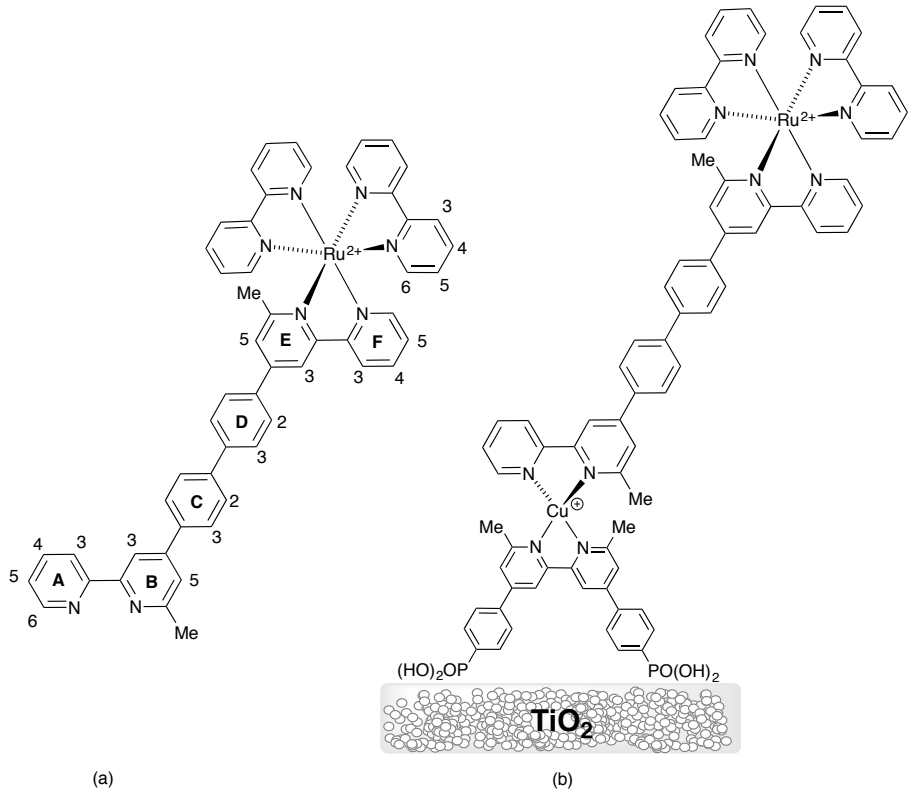

Scheme 6 (a) Structure of $[Ru(bpy)_2(\mathbf{2})]^{2+}$ with atom numbering for NMR assignments. (b) Adsorbed heteroleptic dye $[Cu(\mathbf{4})\{(\mathbf{2})Ru(bpy)_2\}]^{3+}$.

Table 2 Device characteristics of masked DSSCs with dyes $[Cu(\mathbf{4})\{(\mathbf{2})Ru(bpy)_2\}]^{3+}$ and $[Cu(\mathbf{4})(\mathbf{2})]^{+}$.

Dye	J_{SC} / mA cm^{-2}	V_{OC} / mV	*ff* / %	η / %	Relative η / %
$[Cu(\mathbf{4})(\mathbf{2})]^{+}$	3.89	545	72.2	1.53	21.3
$[Cu(\mathbf{4})\{(\mathbf{2})Ru(bpy)_2\}]^{3+}$	4.76	548	67.4	1.76	24.5
N719	15.7	628	72.9	7.17	100

Photoanodes for DSSCs containing the adsorbed dye shown in Scheme 6b were made by functionalizing FTO/TiO_2 with anchoring ligand **4**, then immersing the electrode in a MeCN solution of $[Cu(MeCN)_4][PF_6]$, followed by a dipping cycle in a MeCN solution of $[Ru(bpy)_2(\mathbf{2})][PF_6]_2$. Table 2 gives the device parameters for DSSCs

containing $[Cu(\mathbf{4})\{(\mathbf{2})Ru(bpy)_2\}]^{3+}$ and $[Cu(\mathbf{4})(\mathbf{2})]^{+}$; note that the latter was prepared independently of the DSSC with $[Cu(\mathbf{4})(\mathbf{2})]^{+}$ considered in Table 1, but shows similar device characteristics. Values of V_{OC} are similar for the two dyes, but J_{SC} is enhanced by the introduction of the $\{(\mathbf{2})Ru^{II}(bpy)_2\}$ domain as observed in the *J*–*V* response (Figure 10a). The increased electron injection is consistent with the improved spectral response at both higher and lower energies in the EQE spectrum (Figure 10b). The improvement in the efficiency of the DSSC containing $[Cu(\mathbf{4})\{(\mathbf{2})Ru(bpy)_2\}]^{3+}$ with respect to that $[Cu(\mathbf{4})(\mathbf{2})]^{+}$ probably arises predominantly from the broader absorption range imparted by the ancillary ligand $[(\mathbf{2})Ru(bpy)_2]^{2+}$, and the result encourages us to develop the chemistry of the peripheral ruthenium(II) domain to enhance perfomance further.

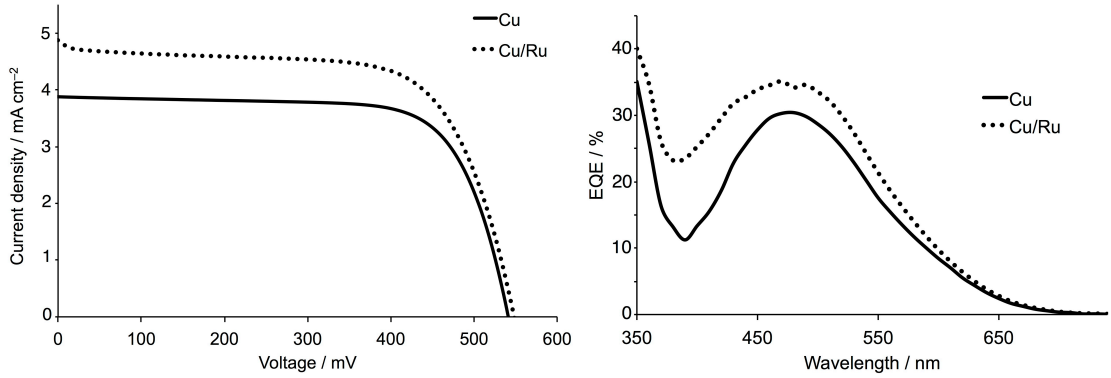

(a) (b)

Figure 10 (a) J–V curves and (b) EQE spectra for DSSCs containing the dyes $[Cu(\mathbf{4})(\mathbf{2})]^{+}$ (solid line) and $[Cu(\mathbf{4})\{(\mathbf{2})Ru(bpy)_2\}]^{3+}$ (dotted line).

4 Conclusions

We have used a new 'surfaces-as-ligands, surfaces-as-complexes' stepwise assembly methodology to prepare a series of dyes containing $\{Cu^{I}(bpy)_2\}$ cores attached to a TiO_2 semiconductor surface through an anchoring ligand and possessing a peripheral metal-

binding domain. Both J_{SC} and V_{OC} increase on going from [Cu(**4**)(**1**)]$^{+}$ to [Cu(**4**)(**2**)]$^{+}$ to [Cu(**4**)(**3**)]$^{+}$. Sequential and alternating treatment of the 'surface-as-ligand' species FTO/TiO_2–**4** with $[Cu(MeCN)_4]^{+}$ and ligand **3** leads to the assembly of first, second and thirds generation dyes $[(\mathbf{4})\{Cu(\mathbf{3})\}_n]^{n+}$ (n = 1, 2 or 3). However, this strategy for increasing the separation between sites of electron injection and hole transporting domain fails to enhance DSSC performance; instead a drop in J_{SC} contributes to poorer overall efficencies for the higher generation dyes. Replacing ancillary ligand **2** in [Cu(**4**)(**2**)]$^{+}$ by $[Ru(bpy)_2(\mathbf{2})]^{2+}$ improves dye perfomance due to the better spectral response of the heteronuclear $[Cu(\mathbf{4})\{(\mathbf{2})Ru(bpy)_2\}]^{3+}$ dye. We are now extending the use of the 'surfaces-as-ligands, surfaces-as-complexes' approach and focusing attention on improved design of the peripheral metal-containing domain for enhanced DSSC performance.

Acknowledgements

The project is supported by the European Research Council (Advanced Grant 267816 LiLo), the Swiss National Science Foundation as part of the NCCR Molecular Systems Engineering, and the University of Basel.

References

[1] Pullerits T, Sundström V. Photosynthetic light-harvesting pigment-protein complexes: toward understanding how and why. Acc Chem Res 1996; 29; 381–389.

[2] Balzani V, Campagna S, Denti G, Juris A, Serroni S, Venturi M. Harvesting sunlight by artificial supramolecular antennae. Solar Energy Mater. Solar Cells, 1995; 38; 159–173.

[3] Ritz T, Damjanović A, Schulten K. The quantum physics of photosynthesis. ChemPhysChem 2002; 3; 243–248.

[4] Sykora M, Maxwell K A, DeSimone J M, Meyer T J. Mimicking the antenna-electron transfer properties of photosynthesis. Proc. Natl. Acad. Sci. 2000; 97; 7687–7691.

[5] Calzaferri G, Pauchard M, Maas H, Huber S, Khatyr A, Schaafsma T. Photonic antenna system for light harvesting, transport and trapping. J. Mater. 2002; 12; 1–13.

[6] Vougioukalakis G C, Konstantakou M, Pefkianakis E K, Kabanakis A N, Stergiopoulos T, Kontos A G, Andreopoulou A K, Kallitsis J K, Falaras P. A ruthenium-based light-harvesting antenna bearing an anthracene moiety in dye-sensitized solar cells. Asian J. Org. Chem. 2014; 3; 953–962.

[7] Konti G, Vougioukalakis G C, Bidikoudi M, Kontos A G, Methenitis C, Falaras P. A Ru(II) molecular antenna bearing a novel bipyridine-acrylonitrile ligand: synthesis and application in dye solar cells. Polyhedron 2014; 82; 12–18.

[8] Cao K, Lu J, Cui J, Shen Y, Chen W, Alemu G, Wang Z, Yuan H, Xu J, Wang M, Cheng Y. Highly efficient light harvesting ruthenium sensitizers for dye-sensitized solar cells featuring triphenylamine donor antennas. J. Mater. Chem. A 2014; 2; 4945–4953.

[9] Lobello M G, Wu K-L, Reddy M A, Marotta G, Grätzel M, Nazeeruddin M K, Chi Y, Chandrasekharam M, Vitillaro G, De Angelis F. Engineering of Ru(II) dyes for interfacial and light-harvesting optimization. Dalton Trans. 2014; 43; 2726–2732.

[10] El-Shafei A, Hussain M, Islam A, Han L. Structure–property relationship of hetero-aromatic-electron-donor antennas of polypyridyl Ru(II) complexes for high efficiency dye-sensitized solar cells. Prog. Photovoltaics 2014; 22; 958–969.

[11] Choi H, Cho N, Paek S, Ko J. Direct evidence of Förster resonance energy transfer for the enhanced photocurrent generation in dye-sensitized solar cell. J. Phys. Chem. C 2014; 118; 16319–16327.

[12] Serroni S, Campagna S, Puntoriero F, Di Pietr C, McClenaghan N D, Loiseau F. Dendrimers based on ruthenium(II) and osmium(II) polypyridine complexes and the approach of using complexes as ligands and complexes as metals. Chem. Soc. Rev. 2001; 30; 367–375.

[13] Bignozzi C A, Argazzi R, Scandola F, Schoonover J R, Meyer G J. Photosensitization of wide band-gap semiconductors with antenna molecules. Solar Energy Mater. Solar Cells, 1995; 38; 187–198.

[14] Bozic-Weber B, Constable E C, Figgemeier E, Housecroft C E, Kylberg W. Evaluation of polynuclear dendrons as photosensitizers for dye-sensitized solar cells. Energy Environ. Sci. 2009; 2; 299–305.

[15] Nazeeruddin M K, Liska P, Moser J, Vlachopoulos N, Grätzel M. Conversion of light into electricity with trinuclear ruthenium complxes adsorbed on textured TiO_2 films. Helv. Chim. Acta 1990; 73; 1788–1803.

[16] Lees A C, Kleverlaan C J, Bignozzi C A, Vos J G. Photophysical properties of TiO_2 surfaces modified with dinuclear RuRu or RuOs polypyridyl complexes. Inorg. Chem. 2001; 40; 5343–5349.

[17] Gholamkhass B, Koike K, Negishi N, Hori H, Sano T, Takeuchi. Adjacent- versus remote-site electron injection in TiO_2 surfaces modified with binuclear ruthenium complexes. Inorg. Chem. 2003; 42; 2919–2932.

[18] McCall K L, Jennings J R, Wang H, Morandeira A, Peter L M, Durrant J R, Yellowlees L J, Robertson N. Dinucear Ru–Cu complexes: Electronic characterisation and application to dye-sensitized solar cells. Eur. J. Inorg. Chem. 2011; 589–596.

[19] Balzani V, Juris A, Venturi M, Campagna S, Serroni S. Luminescent and redox-active polynuclear transition metal complexes. Chem. Rev. 1996; 96; 759–833.

[20] Balzani V, Campagna S, Denti G, Juris A, Serroni S, Venturi M. Designing dendrimers based on transition-metal complexes. Light-harvesting properties and predetermined redox patterns. Acc. Chem. Res. 1998; 31; 26–34.

[21] Malzner F J, Brauchli S Y, Constable E C, Housecroft C E, Neuburger M. Halos show the path to perfection: peripheral iodo-substituents improve the efficiencies of bis(diimine)copper(I) dyes in dye-sensitized solar cells. RSC Adv. 2014; 4; 48712–48723.

[22] Bozic-Weber B, Constable E C, Housecroft C E, Kopecky P, Neuburger M, Zampese J A. The intramolecular aryl embrace: from light emission to light absorption. Dalton Trans. 2011; 40; 12584–12594.

[23] Bozic-Weber B, Chaurin V, Constable E C, Housecroft C E, Meuwly M, Neuburger M, Rudd J A, Schönhofer E, Siegfried L. Exploring copper(I)-based dye-sensitized solar cells: a complementary experimental and TD-DFT investigation. Dalton Trans. 2012; 41; 14157–14169.

[24] Bozic-Weber B, Brauchli S, Constable E C, Fürer S O, Housecroft C E, Wright I A. Hole-transport functionalized copper(I) dye sensitized solar cells. Phys. Chem. Chem. Phys. 2013; 15; 4500–4504.

[25] Bozic-Weber B, Brauchli S Y, Constable E C, Fürer S O, Housecroft C E, Malzner F J, Wright I A, Zampese J A. Improving the photoresponse of copper(I) dyes in dye-sensitized solar cells by tuning ancillary and anchoring ligand modules. Dalton Trans. 2013; 42; 12293–12308

[26] Hewat T E, Yellowlees L J, Robertson N. Neutral copper(I) dipyrrin complexes and their use as sensitizers in dye-sensitized solar cells. Dalton Trans., 2014, 43, 4127–4136.

[27] Bozic-Weber B, Constable E C, Fürer S O, Housecroft C E, Troxler L J, Zampese J A. Copper(I) dye-sensitized solar cells with $[Co(bpy)_3]^{2+/3+}$ electrolyte. Chem. Commun. 2013; 49; 7222–7224.

[28] Brauchli S Y, Bozic-Weber B, Constable E C, Hostettler N, Housecroft C E, Zampese J A. Factors controlling the photoresponse of copper(I) diimine dyes containing hole-transporting dendrons in dye-sensitized solar cells. RSC Adv. 2014; 4; 34801–34815.

[29] Brauchli S Y, Malzner F J, Constable E C, Housecroft C E. Influence of a co-adsorbant on the performance of bis(diimine) copper(I)-based dye-sensitized solar cells. RSC Adv., 2014, revised paper submitted RA-ART-10-2014-012284.

[30] Rao P, Amini M, Li H, Habeeb A G, Knaus E E. 6-Alkyl, alkoxy, or alkylthio-substituted 3-(4-methanesulfonylphenyl)-4-phenylpyran-2-ones: a novel class of diarylheterocyclic selective cyclooxygenase-2 inhibitors. Bioorg. Med. Chem. Lett. 2003; 13; 2205–2209.

[31] Fan C, Wang X, Ding P, Wang J, Liang Z, Tao X. Synthesis, photophysical and iron-sensing properties of terpyridyl-based triphenylamine derivatives, Dyes and Pigments 2012; 95; 757–767.

[32] Li J-H, Higuchi M. Substituent effects on metallo-supramolecular coordination polymers. J. Inorg. Organomet. Polym. 2010; 20; 10–18.

[33] Kubas G J. Tetrakis(acetonitrile)copper(1+) hexafluorophosphate(1–), Inorg. Synth. 1990; 28; 68–70.

[34] Sullivan B P, Salmon D J, Meyer T J. Mixed phosphine 2,2'-bipyridine complexes of ruthenium. Inorg. Chem. 1978; 17; 3334–3341.

[35] Yamamura S, Toda M, Hirata Y. Modified Clemmensen reduction: cholestane. Org. Synth. 1973; 53; 86.

[36] Downard A J, Honey G E, Phillips L F, Steel P J. Synthesis and properties of a tris(2,2'-bipyridine)ruthenium(II) dimer directly coupled at the C4 carbon. Inorg. Chem. 1991; 30; 2259–2260.

[37] Bruker Analytical X-ray Systems, Inc., 2006, APEX2, version 2 User Manual, M86-E01078, Madison, WI.

[38] G. M. Sheldrick, Acta Crystallogr., Sect. A 64 (2008) 112.

[39] I. J. Bruno, J. C. Cole, P. R. Edgington, M. K. Kessler, C. F. Macrae, P. McCabe, J. Pearson, R. Taylor, Acta Crystallogr., Sect. B 58 (2002) 389.

[40] C. F. Macrae, I. J. Bruno, J. A. Chisholm, P. R. Edgington, P. McCabe, E. Pidcock, L. Rodriguez-Monge, R. Taylor, J. van de Streek, P. A. Wood, J. Appl. Cryst., 41 (2008) 466.

[41] Ito S, Murakami T N, Comte P, Liska P, Grätzel C, Nazeeruddin M K, Grätzel M. Fabrication of thin film dye sensitized solar cells with solar to electric power conversion efficiency over 10%. Thin Solid Films 2008; 516; 4613–4619.

[42] Ito S, Chen P, Comte P, Nazeeruddin M K, Liska P, Péchy P, Grätzel M, Fabrication of screen-printing pastes from TiO_2 powders for dye-sensitised solar cells. Prog. Photovoltaics Res. Appl. 2007; 15; 603–612.

[43] Fushimi K, Seo M. An SECM observation of dissolution distribution of ferrous or ferric ion from a polycrystalline iron electrode. Electrochim. Acta 2001; 47; 121-127.

[44] Martin C J, Bozic-Weber B, Constable E C, Glatzel T, Housecroft C E, Wright I A. Using scanning electrochemical microscopy as a tool to examine copper(I) sensitizers for dye sensitized solar cells. J. Phys. Chem. C 2014; 118; 16912–16918.

[45] Brandt W W, Dwyer F P, Gyarfa E D, Chem. Rev. 1954; 545; 959–1017.

[46] Tiecco M, Testaferri L, Tingoli M, Chianelli D, Montanucci M. A convenient synthesis of bipyridines by nickel-phosphine complex-mediated homo coupling of halopyridines. Synthesis 1984; 736–738.

[47] Malzner F J, Brauchli S Y, Schönhofer E, Constable E C, Housecroft C E. To deprotect or not to deprotect: phosphonate ester versus phosphonic acid anchor ligands in copper(I)-based dye-sensitized solar cells. Polyhedron 2014; 82; 116–121.

[48] Mishra A, Fischer M K R, Bäuerle P. Metal-free organic dyes for dye-sensitzed solar cells: From structure-property relationships to design rules. Angew. Chem. Int. Ed. 2009; 48; 2474–2499.

[49] Kroeze J E, Hirata N, Koops S, Nazeeruddin Md K, Schmidt-Mende L, Grätzel M, Durrant J R. Alkyl chain barrier for kinetic optimization in dye-sensitized solar cells. J. Am. Chem. Soc. 2006; 128; 16376–16383.